JOURNAL OF MATERIALS SCIENCE 9 (1974) 1681–1688

Ultrafine oxide powders prepared by electron beam evaporation

Part 1 *Evaporation and condensation processes*

J. D. F. RAMSAY, R. G. AVERY
Chemistry Division, AERE, Harwell, Oxon, UK

Several ultrafine oxide powders (MgO, CaO, Al_2O_3, SiO_2, ZrO_2, CeO_2, U_3O_8) have been prepared by evaporation of bulk oxide with a focused beam of electrons, followed by condensation of the vapour. Rates of evaporation were dependent on the temperature of the heated zone and the corresponding vapour pressure of the oxide, and agreed with those predicted by the Hertz-Langmuir equation. The microstructure of the powders was affected by the pressure and type of gas present during condensation of the vapour. Particles, which were nucleated in the vapour phase, were unagglomerated and had an extremely small size ($\lesssim$ 10 nm) which was dependent on the rate of evaporation; at very low rates, sizes approaching the critical nucleus ($\lesssim$ 3 nm) were attained.

1. Introduction

Ultrafine oxide powders (size $<$ 0.1 μm) have extensive uses, for example, in surface coatings, high density ceramics, dispersion strengthening of metals, pigments, and catalysts. The surface properties and microstructure of such powders are important in many of these applications, and often depend on the method of preparation [1]. Powder production by vapour phase routes has progressed rapidly in recent years, with particular emphasis on plasma processes [2]. These methods can yield unaggregated particles of narrow size distribution and allow a greater control of chemical composition, phase structure, and surface characteristics than is possible with conventional solid state decomposition processes. However, although the technical development of plasma processes has received considerable effort, relatively little attention has been made to study the structure and reactivity of molecular species formed on vaporization, and the mechanism of their condensation [3].

In the present study a novel vapour phase condensation method, for producing ultrafine powders (e.g. oxides, carbides and borides) on an experimental scale is described, in which bulk ceramic is evaporated with a collimated beam of electrons. The evaporation and condensation behaviour of various oxides has been investigated with particular reference to the surface properties and microstructure of the powders so produced.

2. Experimental

2.1. Powder preparation

Powders were prepared by evaporation of bulk oxide with a focused electron beam, from a 1 kW glow discharge gun, A, followed by controlled condensation in a large cube-shaped stainless steel chamber, B (Fig. 1). The gun, developed at AERE [4], had a rotating aluminium cathode, C, which allowed steady operation over long periods; it was connected to the chamber via a narrow water-cooled flight tube, D, which was concentric with two electromagnetic focusing coils, E.

Independent control of both the type and pressure of gas in the gun and chamber were thus achieved. The target, F, consisting of ceramic chips or granules, could be automatically rotated, thus continuously exposing fresh surface for evaporation. Powder was deposited on a water-cooled, nickel-plated brass tube, G, (diameter 0.15 m) surrounding the target; the fluffy deposit which normally formed was readily brushed-off and collected at the end of a run. For oxide preparations, a glow discharge was produced with oxygen at a

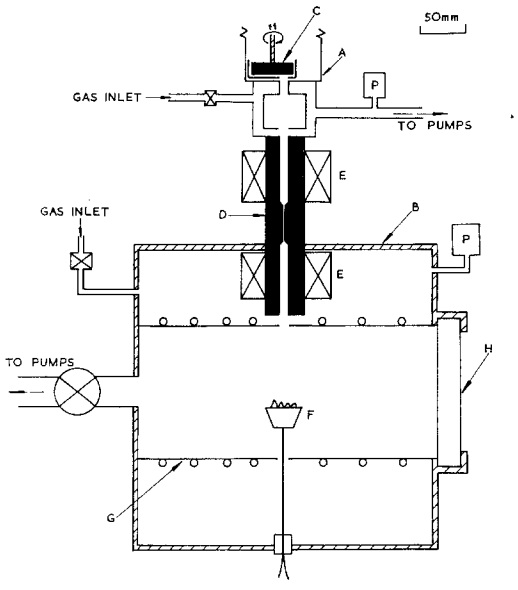

Figure 1 Diagram of electron beam gun and evacuable chamber.

pressure of 7 N m^{-2} with a voltage in the range 15 to 30 kV. The type of gas and pressure in the chamber markedly affected the properties of the powders, as will be discussed; however, oxygen, at pressures in a range up to $\sim$ 100 N m^{-2}, was normally employed.

2.2. Temperature measurement

The "brightness temperature" of the heated zone was measured with a disappearing filament optical pyrometer, after a correction had been made for absorption by the window, H (cf. Fig. 1) (which was made of thick lead glass to reduce secondary X-ray emission) of the chamber. Published values of spectral emissivity, $\epsilon_{0.65\mu m}$ were used to calculate true surface temperatures. These were taken from the data of Noguchi [5] for opaque specimens of calcia, alumina and zirconia, at temperatures close to the melting point. There was more uncertainty in ϵ for the two oxides used in transparent form (Vitreosil®, periclase); however, for similar conditions, values of $\sim$ 0.2 have been reported [6].

2.3. Powder characterization

Specimens for electron microscopy (JEM-7) were generally prepared *in situ* by deposition of powder onto a carbon film coating the microscope grids; the thickness of deposits was controlled with a shutter, operated from outside the chamber.

Crystallite sizes were calculated from X-ray line half widths, measured with a diffractometer. (A Gaussian line profile was assumed and standard corrections were made for the instrumental broadening and doublet overlap of the $K\alpha_1$ and $K\alpha_2$ lines [7].)

3. The evaporation process

3.1. Experimental rates of evaporation

Several ceramic oxides were evaporated in oxygen with an electron beam (at accelerating voltages of 25 to 28 kV) focused to a spot of $\sim$ 3 mm diameter.

The rate of evaporation decreased with the refractoriness of the oxide (Table I), the trend being more dependent on vapour pressure than melting point (Table II) however. Since the sublimation of oxides at high temperature frequently involves simultaneous dissociation (Table II), these values of v.p. correspond to the total partial pressures of all vapour species, as derived experimentally and thermodynamically from free energy data [8].

3.2. Estimation of maximum theoretical evaporation rates

The maximum rate of evaporation from a heated surface can be related to its equilibrium vapour pressure, P_{eq}, given by the Hertz-Langmuir equation [9]:

$$J = (2\pi MRT)^{-\frac{1}{2}} P_{eq}\alpha \qquad (1)$$

where J is the flux from the surface in moles per unit area per unit time, M is the molecular weight of the vapour, and α is the evaporation coefficient (which can be assumed to be unity for a smooth surface of a solid close to its m.p. *in vacuo* < 1 N m^{-2}).

In the temperature range of interest (2000 to 3000 K), silica and magnesia are known to dissociate predominantly by the following reactions on evaporation:

$$MgO \rightarrow Mg + \tfrac{1}{2}O_2$$
$$SiO_{2,(liq)} \rightarrow SiO_{(gas)} + \tfrac{1}{2}O_2 .$$

Since published values of free energy, ΔG, for these reactions are available for different temperatures [10, 11] we can calculate the evaporation rates as follows.

For congruent evaporation, the fluxes of each species are determined by stoichiometry as

$$J_{Mg(max)} = 2J_{O_2,(max)} \text{ and}$$
$$J_{SiO(max)} = 2J_{O_2(max)} .$$

Now

$$P_{Mg(eq)} \cdot P^{\frac{1}{2}}_{O_2(eq)} = \exp \frac{-\Delta G^0}{RT} \quad (2)$$

where ΔG^0 is the free energy of the vaporization reaction. From Equations 1 and 2 we then have

$$J_{Mg(max)} = J_{MgO(max)} = \left(\frac{2^{\frac{1}{2}} \exp(-\Delta G^0/RT)}{M^{\frac{1}{2}}_{Mg} \cdot M^{\frac{1}{2}}_{O_2}}\right)^{2/3} \frac{1}{(2\pi RT)^{\frac{1}{2}}} \cdot \quad (3)$$

similarly it can be shown that

$$J_{SiO(max)} = J_{SiO/(max)} = \left(\frac{2^{\frac{1}{2}} \exp(-\Delta G^0/RT)}{M^{\frac{1}{2}}_{SiO} \cdot M^{\frac{1}{2}}_{O_2}}\right)^{2/3} \frac{1}{(2\pi RT)^{\frac{1}{2}}} \cdot \quad (4)$$

Values of J_{max} are tabulated below (Table III) for different temperatures, together with the appropriate values of $-\Delta G$.

A more approximate calculation, made by inserting the total partial pressure (of all the evaporating species), at a given temperature, into Equation 1, gives evaporation rates as shown in Fig. 2. Experimentally determined rates of evaporation (from Table I and the more extensive data for magnesia, of Table IV) are also plotted and show good accord. Thus although the temperature and area ($\sim$ 3 mm diameter) of the heated zone are somewhat uncertain, these results do indicate evaporation coefficients, α, close to unity as assumed.

3.3. Efficiency of vaporization process

The heats of sublimation, ΔH_e, of solid refractory oxides to gaseous elements in groups II to IV lie in the range 400 to 800 kJ mol^{-1} [12]. The energy consumption for vaporization of magnesia (ΔH_e = 500 kJ mol^{-1}) would be 5.5 kWh kg^{-1}, compared with the experimental figure of 66 kWh kg^{-1} for example. Thus the energy utilization is $\sim$ 10%, and considerably less for alumina and zirconia. The major losses, which have been assessed previously [13], result from electron scattering, both in the beam path and at the bombarded zone. This apparently low efficiency

TABLE I Typical experimental data for oxide evaporation

Oxide	Input power (kW)	Oxygen pressure in chamber (kN m^{-2})	Target temperature* (K $\times$ 10^{-3})		Evaporation rate (g h^{-1})	Evaporative flux per unit area† (mol m^{-2} sec^{-1})	Overall evaporation efficiency (kWh kg^{-1})
			(i)	(ii)			
Silica	0.75	0.03	2.2	2.6 (0.2)	53	35	14
Ceria	1.00	0.03	2.3	2.3 (0.8)	20	4.6	50
Magnesia	1.00	0.03	2.3	2.8 (0.2)	15	15	66
Calcia	1.10	0.05	2.6	2.6 (0.9)	6.6	4.6	170
Alumina	1.08	0.04	2.8	2.8 (1.0)	5.4	2.1	200
Zirconia	1.38	0.05	2.9	3.0 (0.8)	5.5	1.7	250

*(i) denotes "brightness" temperature, (ii) true surface temperature, calculated for $\epsilon_{0.65\mu m}$ quoted in parenthesis.
†Diameter of heated zone is $\sim$ 3 mm.

TABLE II Vapour pressures of oxides

Oxide	Melting point (K)	Vapour pressure (N m^{-2}) at temperature (K $\times$ 10^{-3})			Predominant vapour composition (neutral conditions)
		2.0	2.5	3.0	
SiO_2	2001 (cristobalite)	6	1 $\times$ 10^3	7 $\times$ 10^4	SiO, SiO_2
MgO	3070	0.23	80	4 $\times$ 10^3	elements
CaO	2853	1.5 $\times$ 10^{-2}	9.3	5.3 $\times$ 10^2	elements
Al_2O_3	2290	6.1 $\times$ 10^{-3}	1.2	1.6 $\times$ 10^2	elements, Al_2O, AlO
ZrO_2	2970	4.2 $\times$ 10^{-5}	1.3 $\times$ 10^{-1}	33	ZrO, ZrO_2

TABLE III Free energy changes for dissociation reactions during evaporation of silica and magnesia

Temperature (K)	Free energy change, $-\Delta G$(kJ mol^{-1})		Maximum evaporation rates, J_{max} (mol m^{-2} sec^{-1})	
	$SiO_{2(l)} \rightarrow SiO_{(g)} + \frac{1}{2}O_2$	$MgO_{(s)} \rightarrow Mg_{(g)} + \frac{1}{2}O_2$	$J_{max(SiO2)}$	$J_{max(MgO)}$
2000	270	320	3.96×10^{-2}	7.80×10^{-3}
2500	150	210	12.7	2.77
3000	43	92	2.4×10^{3}	1.99×10^{2}

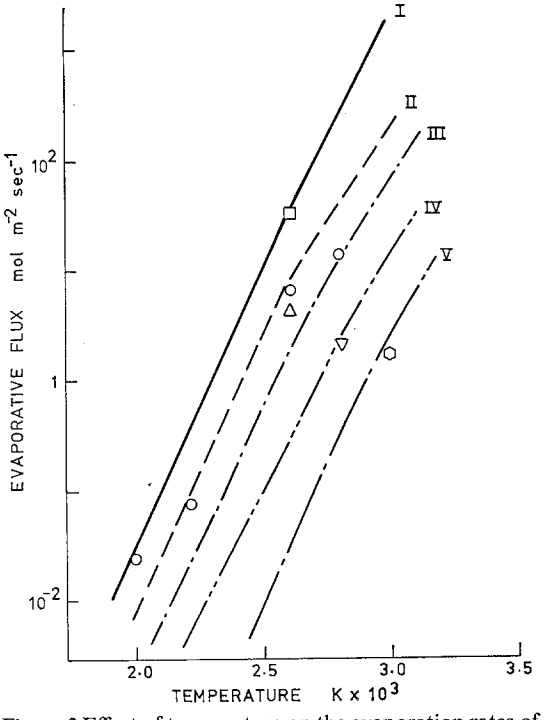

Figure 2 Effect of temperature on the evaporation rates of different oxides, calculated from free energy and vapour pressure data. Symbols denote experimental values. I and □, silica; II and ○, magnesia; II and △, calcia; IV and ▽, alumina; V and ◇, zirconia.

is nevertheless comparable to that reported for currently developed plasma processes. Values for silica and magnesia, for example, are close to those reported by Sayce and Selton [14] (14 and 35 kWh kg^{-1} respectively) for powder production by ceramic evaporation with a 30 kW d.c. plasma jet in a liquid-wall furnace. Furthermore, this latter process is claimed to be considerably more efficient than methods employing R.F. plasmas. A marked increase in the efficiency of the present process would be expected for a larger scale of production, employing guns of greater power operating at higher voltages. The effect of accelerating voltage, is illustrated (Table IV) by the efficiency of evaporation (kg kWh^{-1}) of magnesia which was increased ~ 10-fold on increasing the voltage from 15 kV (runs 25 and 30) to 30 kV (runs 26 and 31).

3.4. Conditions for vapour phase nucleation

The type and pressure of gas in the chamber during evaporation markedly affected the nature of the deposited powder, especially for those oxides (MgO, CaO) which dissociated on evaporation. Powders deposited on the water cooled collector from an oxygen atmosphere at low pressure (< 20 N m^{-2}) were more adherent and had a higher bulk density than the fluffy deposits produced at pressures in the range 30 to 60 N m^{-2}. In a helium atmosphere, dense deposits were even produced at pressures > 40 N m^{-2}. These differences are illustrated in the electron micrographs of silica and magnesia, Figs. 3 and 4, deposited (on a carbon film *in situ*) at the extremes of oxygen pressure. At high pressure discrete particles (size ~ 10 nm) were produced, whereas at low pressures a continuous coherent structure was formed. This latter possibly consisted of aggregates of extremely small particles (< 2 nm) although the structure could not be fully defined due to the limitation of microscope resolution. The effect of gas pressure varied with the oxide and was least marked for silica. However, for oxides which dissociated to atoms on evaporation (MgO, CaO), hard adherent deposits were formed at any pressure in atmospheres (He, N_2, H_2) free of oxygen (P_{O_2} < 0.2 N m^{-2}). These were often brown or black, presumably as a result of non-stoichiometry. They also contained extremely small micropores (radius < 2 nm), in contrast to the non-porous unagglomerated powders of low bulk density to be described in Part II. This is evidenced by the nitrogen adsorption isotherm of magnesia deposited in helium (33 N m^{-2}) in Fig. 5. Water was desorbed from micropores on increasing the degassing temperature from 423 to 673K, thus increasing the N_2 uptake at p/p_0

TABLE IV Properties of magnesia powders prepared at different rates of evaporation

Run no.	Input power (kW)	Chamber pressure (P_{O_2}, N m^{-2})	Brightness temperature (K $\times 10^{-3}$)	Corrected temperature (K $\times 10^{-3}$)	Evaporation rate (g h^{-1})	S_{BET} (m^2 g^{-1}*)	Particle† size (nm)		X-ray crystallite size (nm)	
							(i)	(ii)	200	220
26	1.07	50	2.2	2.6	6.5			15	13	12
31	0.56	40	2.2	2.6	3.0				11	11
25	0.30	50	1.8	2.2	0.08	270	6.2		4.9	4.1
30	0.30	50	1.7	2.0	0.03	360	4.6	5	4.1	4.0

*Denotes specific surface area based on dry weight.
†Particle size from (i) S_{BET}, and (ii) electron microscopy.

< 0.4, and leading to an apparent increase in S_{BET} from 34 to 140 m^2 g^{-1}.

The properties of the powder deposits were probably determined by the type of nucleation process. The recombination of molecules (or atoms) in the vapour phase to form dimers and trimers etc (which subsequently leads to vapour phase nucleation) can be visualized as a process involving a three-body collision between two vapour species and a gas molecule to remove the excess energy. A quantitative treatment of prenucleation kinetics for a system involving trimolecular collisions of oxide vapour molecules of uncertain structure is evidently very difficult, and the following is only a crude qualitative approach. The problem can be tackled [15] by estimating the lifetime, τ, of a bimolecular complex resulting from a collision of two vapour molecules; this would be dependent on the time the molecules were within some small distance of

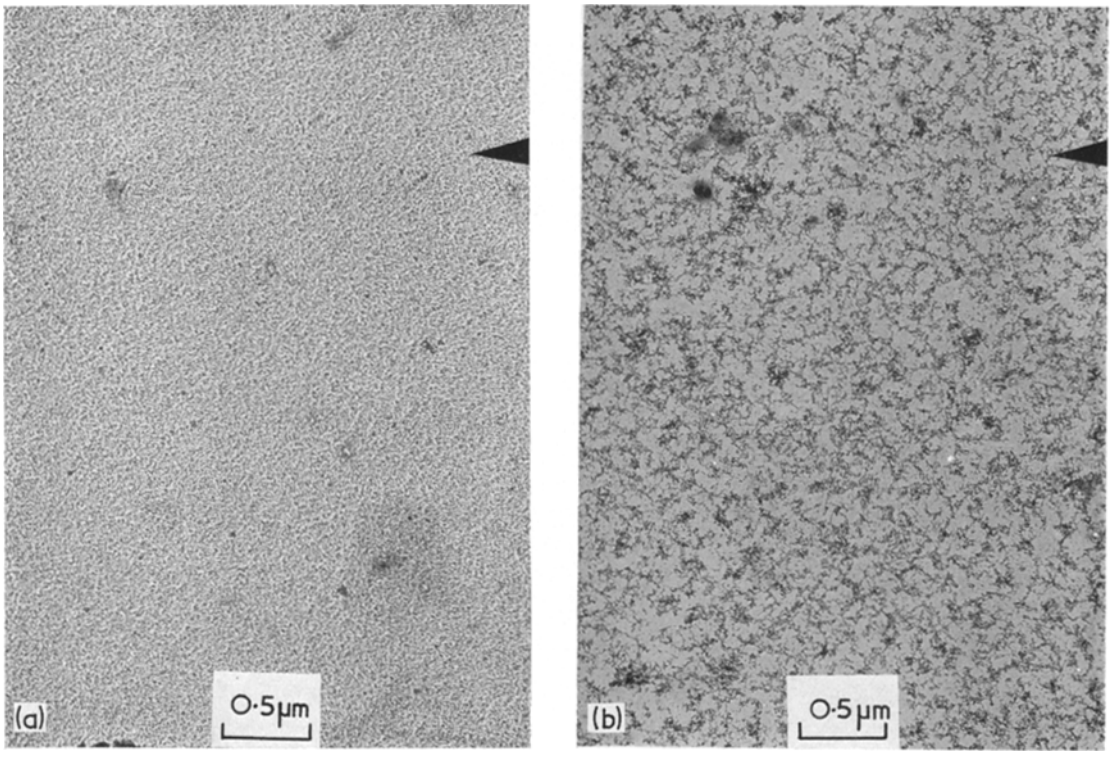

Figure 3 Electron micrographs of silica deposited *in situ* from an oxygen atmosphere of (a) low pressure (15 N m^{-2}) and (b) high pressure (53 N m^{-2}).

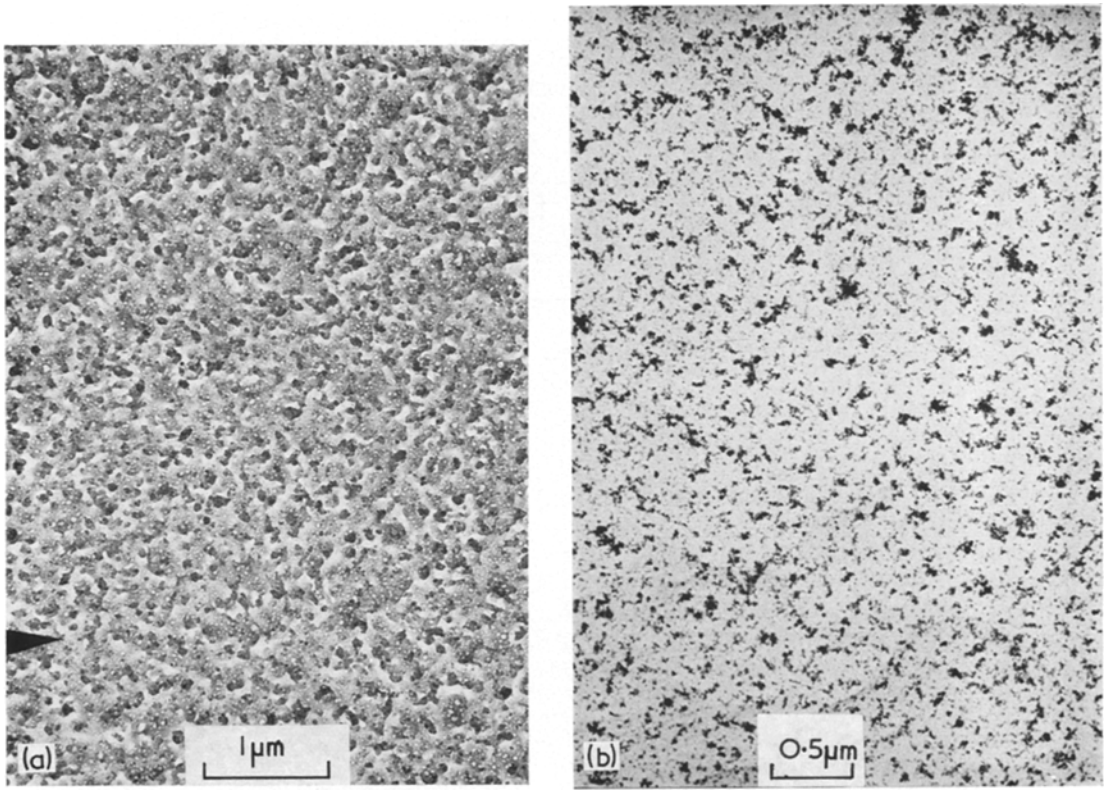

Figure 4 Electron micrographs of magnesia deposited *in situ* from an oxygen atmosphere of (a) low pressure (7 N m^{-2}) and (b) high pressure ($\sim$ 50 N m^{-2}).

interaction, δ. (It is normal to assume $\delta \sim 0.1$ nm which would correspond to a value τ of 10^{-12} to 10^{-13} sec.) Denoting the number concentration of the two vapour molecules as N_1 and N_2 and their average diameter as σ_{12}, the number concentration N_{12} of bimolecular species at equilibrium is given by:

$$N_{12} = N_1 N_2 \,.\, 4\pi\delta\sigma_{12}^2 \,. \qquad (5)$$

The rate of collisions, Z, of gas molecules with bimolecular complexes is

$$Z = N_g \,.\, N_{12}\pi \left[\frac{\sigma_c + \sigma_g}{2}\right]^2 \left(\frac{8kT}{\pi\mu}\right)^{\frac{1}{2}} \qquad (6)$$

where N_g is the number concentration of gas molecules, at temperature T, σ_c and σ_g the diameters of the complex and gas molecules and μ the reduced mass of the complex and gas molecule $[1/\mu = (1/m_c) + (1/m_g)]$. From Equations 5 and 6 we obtain:

$$Z = 2\sqrt{2}\,\pi^{3/2} N_1 \,.\, N_2 \,.\, N_g (\sigma_c + \sigma_g)^2 \sigma_{12}^2 \,\delta(kT)^{\frac{1}{2}} \mu^{-\frac{1}{2}} \,. \qquad (7)$$

Thus Z is directly proportional to N_g (namely, the gas pressure) and increases with the molecular diameter of the gas. This accounts for the different pressure thresholds for helium and oxygen ($\sim$ 20 and $\sim$ 50 N m^{-2} respectively) above which "fluffy" powders were obtained. Furthermore the collision diameter, σ_c, of an oxide molecule can be crudely estimated if Z is assumed identical at these two different pressures. Thus

$$2(\sigma_c + \sigma_{He})^2 = (\sigma_c + \sigma_{O_2})^2$$

which taking σ_{He} and σ_{O_2} to be 0.22 and 0.36 nm respectively gives $\sigma_c = 0.35$ nm – a realistic value considering the gross approximations involved. Equation 7 also predicts a greater probability of vapour phase condensation as the concentration of vapour species (N_1 and N_2) increases (i.e. the rate of evaporation) and also as the size of the vapour molecule becomes larger, and would explain why the deposits of silica were least sensitive to gas pressure in contrast to magnesia and calcia.

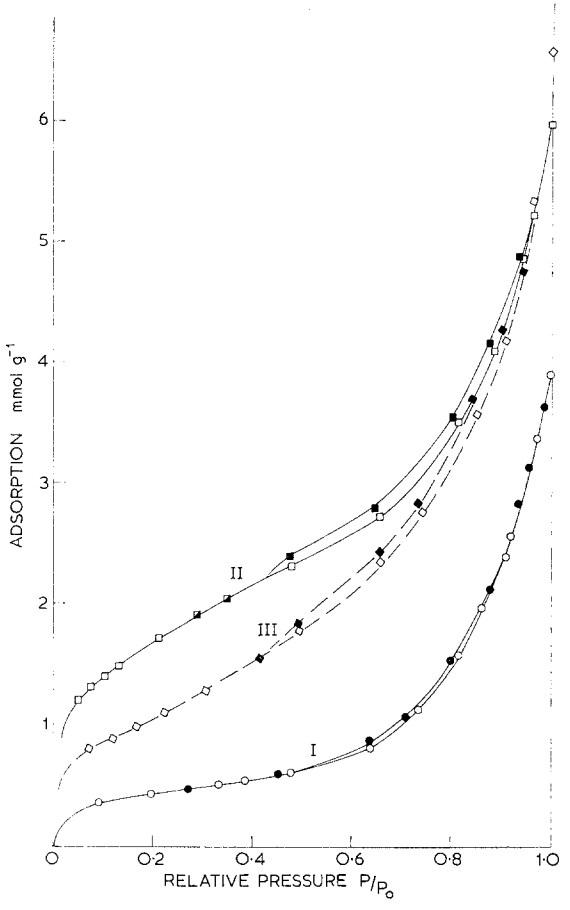

Figure 5 Adsorption isotherms of nitrogen at 77 K for magnesia powder deposited in helium (p_{He} = 33 N m^{-2}). After pumping: I, at 423 K; II at 673 K; III at 973 K. Solid symbols denote desorption.

A chemical vapour deposition process probably occurs when MgO and CaO are evaporated in low (P_{O_2} < 10 N m^{-2}) partial pressures of oxygen. The species which nucleated heterogeneously at the substrate under such conditions were reactive and combined chemically with silica or pyrex glass surfaces. Control of the stoichiometry of powders nucleated in the vapour phase was also possible by reaction of vapour species with oxygen. Thus the stoichiometry of uranium oxide powder could be varied from UO_2 to UO_3 by evaporation of UO_2 into either an inert or oxidizing atmosphere as described in Part II.

3.5. Conditions affecting particle size

For all preparations the particle size was confined to a relatively narrow range below ~ 10 nm, and showed little dependence on the type of oxide produced, with the exception of U_3O_8 which will be discussed in Part II. This feature can be ascribed to a high supersaturation of vapour in the immediate vicinity of the heated source, which results in a rapid formation of a large number of nuclei, and thus a consequent depletion of the vapour concentration [16]. The growth of these nuclei is thus restricted as they diffuse into the surrounding volume of the chamber. The size is, therefore, determined by three factors: the rate of vapour production (evaporation rate), the degree of supersaturation and the rate of diffusion of nuclei away from the source.

The dependence of the crystallite size of magnesia powders on the rate of evaporation tends to support such a mechanism. The size, determined for the 200 and 220 planes from X-ray line broadening (Table IV) diminished as the rate of evaporation decreased until a size of ~ 4 nm was reached; this apparent lower limit was probably imposed by surface and free energy considerations. Moreover the crystallite size of specimens collected at distances which varied from 50 to 200 nm from the source showed no significant difference, confirming that crystal growth was restricted to a small volume of vapour surrounding the heated zone.

The lower limit in particle size of all powders is probably determined by the size of the critical nucleus. The number of molecules in a critical nucleus of water at 300 K has been estimated by Russel *et al.* [17] to be ~ 100. A crude application of this value to magnesia gives a critical size of ~ 2 nm, which considering the above assumptions, and the general limitations in the determination of crystallite size by line broadening, is in reasonable agreement with the smallest size observed with MgO and all other oxide powders produced.

4. Conclusions

1. Oxide powders with an exceptionally small particle size (< 20 nm), can be produced by evaporating bulk oxide with a focused electron beam followed by vapour phase condensation.

2. The rate of evaporation is dependent on (a) the temperature of the heated zone and (b) the vapour pressure of the particular oxide. Experimentally determined rates are in reasonable accord with those predicted by the Hertz-Langmuir equation.

3. The efficiency of evaporation, with an

electron beam gun operating at ~ 30 kV and ~ 1 kW, is in the range 14 to 250 kWh kg^{-1} depending on the volatility of the oxide; it could be substantially improved with guns of increased power operating at higher voltage. The efficiency for SiO_2 and MgO evaporation even with a 1 kW gun is, however, comparable to that of d.c. arc plasma methods of powder production operating at 30 kW.

4. Nucleation of oxide vapour species occurs predominantly in the vapour phase when the pressure of gas in the condensation chamber is high ($\gtrsim 30$ N m^{-2}); at low pressures (< 10 N m^{-2}), when the mean free path is long, heterogeneous nucleation at the substrate results in adherent porous deposits.

5. The extremely small particle size of the powders can be ascribed to a very rapid nucleation and subsequent restriction in crystal growth caused by a depletion of vapour species. At low evaporation rates particles sizes approaching the critical nucleus ($\lesssim 3$ nm) are attained.

Acknowledgements

We are indebted to Dr R. A. Dugdale, for advice and information relating to glow discharge electron beams, and who, together with Mr P. A. Thackeray, was responsible for the design and construction of the electron gun.

References

1. W. E. KUHN (Ed.) in "Ultrafine Particles" (John Wiley, New York, 1963) p. 3 *et seq.*
2. B. WALDIE, *Chem. Eng.* (259) (1972) 92.
3. See for example, J. M. COULSON, *et al.* (Eds.) in "High Temperature Processes" (Science Research Council, London, 1971).
4. J. T. MASKREY and R. A. DUGDALE, *J. Phys. E* **5** (1972) 881.
5. T. NOGUCHI, in "Advances in High Temperature Chemistry", Vol. 2, edited by L. Eyring (Academic Press, New York, 1969).
6. P. L. HAUST, in "Temperature, its Measurement and Control in Science and Industry", Vol. 3, Part 2, edited by C. M. Herzfeld (Rheinbold, New York, 1962) p. 489.
7. H. P. KLUG and L. E. ALEXANDER, "X-ray Diffraction Procedures" (John Wiley, New York, 1967) p. 491.
8. M. S. CHANDRASEKHARAIAH, in "The Characterization of High Temperature Vapours", edited by J. L. Margrave (John Wiley, New York, 1967) p. 495.
9 A. W. SEARCY, in "Chemical and Mechanical Behaviour of Inorganic Materials", edited by A. W. Searcy, D. V. Ragone and U. Colombo (John Wiley, New York, 1970) p. 107.
10. G. DE MARIA, *ibid* p. 64.
11. H. L. SCHICK, *Chem. Rev.* **60** (1960) 331.
12. R. J. ACKERMANN and R. J. THORN, in "High Temperature Technology" (IUPAC/Butterworths, London, 1964) p. 141.
13. R. G. AVERY and J. D. F. RAMSAY, unpublished work.
14. I. G. SAYCE and B. SELTON, in "Special Ceramics", edited by P. Popper (British Ceramic Research Association, 1972) p. 157.
15. L. S. KASSEL, "The Kinetics of Homogeneous Gas Reactions" (Chemical Catalogue Co, New York, 1932) p. 75.
16. A. W. ADAMSON, "Physical Chemistry of Surfaces" (John Wiley, New York, 1960) p. 288.
17. K. C. RUSSEL, J. LOTHE and G. M. POUND, in "Condensation and Evaporation of Solids", edited by E. Rutner, P. Goldfinger and J. P. Hirth (Gordon and Breach, New York, 1964) p. 503.

Recieved 9 April and accepted 1 May 1974.